Numerical prediction of reinforced concrete exterior wall response to blast loading

X. Q. Zhou and H. Hao*

School of Civil & Resource Engineering, the University of Western Australia,

35 Stirling Highway, Crawley WA 6009, Australia

Abstract

It is of interest to know the response of the unretrofitted reinforced concrete exterior walls under blast loading because some infrastructures might be targets of terrorist attack. Detailed numerical simulation and analysis of a typical concrete wall under different blast loads is presented in this study. The concrete material model used in the study includes a dynamic plastic damage model, a modified damage dependent piece-wise Drucker-Prager strength envelope, and a nonlinear equation of state considering the heterogeneity and porosity of concrete materials. The strain rate effect on tensile and compressive strength is considered separately. The concrete damage is based on Mazars' damage model, which combines tensile and compressive damage. The present numerical model was calibrated first by comparing the numerical results with laboratory blast test results of reinforced concrete slabs. The calibrated model is then employed to simulate the response of a typical reinforced concrete exterior wall under blast loads. TNT charge weights corresponding to some typical terrorist bombs, that is, from 10kg to 5000kg, are considered. In terms of different TNT charge weights, the responses of the reinforced concrete wall at different stand-off distances are simulated. Based on the numerical results, critical curves that relate damage levels with the explosion conditions are derived. The safe stand-off distances to resist different terrorist bombing scenarios are suggested.

Keywords: Blast loads; Reinforced concrete wall; Numerical simulation; Material model

* Corresponding author. Tel.: +61-8-6488-1825; fax: +61-8-6488-1044.
E-mail address: hao@civil.uwa.edu.au (H. Hao)

1. Introduction

Some infrastructures, such as government buildings and embassy buildings, or even commercial buildings and residential buildings, might be target of terrorist attack. Terrorist bombing attacks in Oklahoma City, New York City, Saudi Arabia, Kenya, and Tanzania are grim examples of the massive damages to civilian lives and the structures resulting from such activities (Mosalam and Mosallam, 2001). In response to this growing concern, the protection level of some existing buildings against blast loading may need to be evaluated and some new buildings may need to be designed to get certain protection. Some standards (DOD, 2002) and the design methods (TM5-1300, 1990, DOD, 2005) were developed recently to analyze structure response to blast loads, and to assess structural performance with respect to blast weight and stand-off distance. For example, DOD (2002) provides minimum stand-off distances based on the required level of protection. If the minimum stand-off distances are met, conventional construction techniques can be used with some modifications. If the minimum stand-off cannot be achieved, the building must be hardened to get the required level of protection. The stand-off distance given in DOD (2002) provides a quick assessment of structural safety to blast loads. However, the primary drawback is that the damage level is only vaguely defined. It is not clear if 'damage' means collapse of the structure, or collapse of the infill walls, or formation of cracks on the infill walls, or other type of structure or structural component failure. TM5-1300 (1990) includes step-by-step analysis and design procedures for structures to resist the effects of explosions. It appears to be the most widely used publication by both military and civilian organizations for designing structures to prevent the propagation of explosion and to provide protection for personnel and valuable equipment. The analysis method in TM5-1300 can be used to approximately estimate structural responses and damage. But the method is mainly based on the Single Degree of Freedom (SDOF) approach, which cannot give a reliable prediction of local structure damage. To obtain more the accurate response of structures or structure members, detailed analysis than a SDOF approach is often necessary.

In a blast event, the two parameters that most directly influence the blast environment are the bomb's charge weight and the stand-off distance. In a design or analysis procedure, normally the dynamic loading (pressure and impulse) is determined by these two parameters, and then the response of the structure can be analyzed. In association with the pressure and impulse, the widely used way to assess structure damage

is P-I curve (Pressure-impulse curves corresponding to different damage level) (Ambrosini et al., 2005). A P-I curve can be obtained from a simple SDOF analysis, complicated numerical simulations (Lan and Crawford, 2003), or field blast tests. Recently, a range-to-effect chart (FEMA428, 2008) is also used to indicate the distance (or stand-off) to which a given size bomb will produce a given effect. This type of chart can be used to directly display the blast response of a building component at different level of protection.

Current damage assessment methods usually simplify a structure to a SDOF model (Naito and Wheaton, 2006, Morison, 2006, Li and Meng, 2002). In Naito and Wheaton (2006)'s work, a SDOF modelling and a static finite element pushover analysis were combined to calculate the blast resistance of an existing shear wall subjected to an external explosion. P-I curves were obtained for the shear wall. Morison (2006) reviewed many available SDOF methods on reinforced concrete flexural members (walls and slabs) and revised some of the parameters. Based on a SDOF model, Li and Meng (2002) analyzed the characteristics of P-I curves for various descending pulse loads. The SDOF analysis is relatively straightforward and also provides an overall assessment of the structure response to blast loads. However, a SDOF approach may yield unreliable predictions because it cannot capture the coupling between the shear and flexural failure modes, it cannot capture the localized failure of the structure, and the damage criterion based on displacement response of the SDOF model is very difficult to be accurately defined (Lan and Crawford, 2003).

With the rapid development of computer technology and the advancement of numerical techniques, it makes the predictions of the concrete structure damage to blast loads through computer simulation viable (Riedel et al., 1999, AUTODYN, 2005). However, the reliability of the computer simulation results greatly depends on the dynamic material model. Many research works have been done to analyze the behaviour of concrete structures under different loading conditions. Based on static tests, many static strength criteria have been proposed in the past (Pinto, 1996, Chen and Chen, 1975, Chen, 1982, Kotsovos and Newman, 1978, Ottesen, 1977). From dynamic experimental results, it has been found that both the tensile strength and the compressive strength are highly dependent on the strain rate, i.e., the strain rate effect (Bischoff and Perry, 1991, Fu et al., 1991, Malvar and Ross, 1998, Wibl and Schmidt-Hurtienne, 1999, Schuler et al., 2006). The effect of strain rate on the concrete compressive and tensile

strength is typically represented by a parameter, namely the Dynamic Increase Factor (DIF). It is a ratio of the dynamic-to-static material constants versus strain rate. Some material models have been proposed to calculate concrete structural response to highly dynamic loads (Riedel et al., 1999, Holmquist and Johnson, 1993, Espinosia et al., 1998, Malvar et al.,1997, Zhou et al., 2005, Gebbeken and Ruppert, 2000). In 1993, Johnson and Holmquist (2003) developed a brittle damage concrete model used in hydrocodes. Based on this model, RHT model (Riedel at al., 1999) was developed in 1999. The yield and failure surfaces were improved by considering the stress deviator tensor J_3 .The shape in the deviatoric plane is based on the static Willam-Warnke model. In 2000, Gebbeken and Ruppert (2000) developed a high-dynamic material model for concrete which is also derived on the basis of the Johnson-Holmquist model. In their model, a shape function was adopted to define octahedral stresses in the deviatoric plane; the strain rate effect and the damage variable had been improved. Recently, Leppänen (2006) improved the RHT model by using a different DIF for tension and a bi-linear crack softening law. In 2002, Gatuingt and Pijaudier-Cabot (2002) developed a damage visco-plastic model for concrete to consider the interaction between the spherical and deviatoric response. At the same time, meshfree method, such as SPH, has also been used to model concrete response under blast loading (Rabczuk and Eibl, 2003).

Similar to those Johnson-Holmquist based models, the authors (Zhou et al., 2008) developed a simple plastic damage material model and incorporated the model to a hydrocode AUTODYN (2005). In the model, the strength criterion is a damage-based modified Drucker-Prager model, a circle is used in the deviatoric plane to simplify the strength criterion; four sets of static-based experimental results were used to determine the meridian plane; the damage model adopted is based on Mazars' damage model; different DIFs are employed to model the strain rate effect in tension and compression state to match the available experimental results. 3D simulations of RC slab responses to blast loads (Zhou at al., 2008) were carried out by using the model. The comparison between the numerical results with the test results showed that the concrete material model yielded reasonable prediction of RC slab damage to blast loads.

In some buildings, the reinforced concrete (RC) wall is a common structural member. It is of interest to understand the behaviour of the RC walls under blast loading. The objective of the present study is to obtain a range-to-effect chart similar to that in (FEMA428, 2008) for RC walls. In the present study, the calibrated concrete material model together with AUTODYN is used to predict the behaviour of a typical

solid RC exterior wall under blast loading. According to FEMA428 (2008), the explosive weight in a terrorist bombing can be divided into four subcategories, that is, luggage bomb, automobiles bomb, vans bomb and trucks bomb. The TNT weight in a luggage bomb is less than 50kg. Automobile bomb is from 50kg to 200kg TNT equivalent. The TNT equivalent charge weight in a van bomb is from 200kg to 2000kg. The large scale truck bombs typically contain 2000kg or more of TNT equivalent. According this classification, different TNT charge weights, i.e., 10kg, 18kg, 25kg, 50kg, 100kg, 200kg, 500kg, 1000kg, 2000kg and 5000kg, are selected as typical charge weights for the above mentioned four subcategories. In terms of these different TNT charge weights, the responses of the RC wall at different stand-off distances are numerically simulated. According to the numerical results, critical curves related to different damage conditions are suggested and then safe stand-off distances for different terrorist bombing scenarios are determined.

2. Concrete material model

In the present study, the modified Drucker-Prager plastic damage model developed in our previous work (Zhou at al., 2008) is used. In the model, the stress tensor is separated into the hydrostatic tensor and the deviatoric tensor. The hydrostatic stress tensor controls the change of concrete volume and the deviatoric stress tensor controls the shape deformation. Tensile and compressive DIFs are adopted to amplify the tensile yield strength and the compressive yield strength with the strain rate.

For the hydrostatic tensor, the hydrostatic pressure p is often related to the density ρ (or volume v) and the internal energy e through an Equation of State (EOS),

$$p = f(\rho, e) \tag{1}$$

Porous EOS has been widely used in many models (Riedel et al., 1999, Holmquist and Johnson, 1993, Gebbeken and Ruppert, 2000). Typically the pressure-density response for a porous EOS can be separated into three response regions. The first region is linear elastic. The second region is referred to as the transition (or compaction) region. In this compaction region, concrete is assumed to be compacted gradually to convert to a granular kind of material. The third region is the fully compacted region when the pressure reaches a certain value. In this region, the air voids are

completely removed from the material. Gebbeken et al. (2006) specially designed detonation tests and flyer-plate-impact test to analyze the property of EOS for concrete. Typical Pressure-density curve is shown in Figure 1 (Gebbeken et al., 2006). The second region given in Figure 1 is a "best-fit" of the pressure-density data. In the present model, Hermann(1969)'s P-α model is adopted to model the second region and the polynomial EOS is adopted to model the third region. The definition and selection of the parameters used in the EOS can be found in our previous work (Zhou et al., 2008). The constants used are listed in Table 1.

The deviatoric stress tensor is governed by a damage-based yield strength surface. Before the stress state reaches the yield criterion, the concrete material is assumed to be elastic. The incremental form of the Hooke's law is as follows

$$\Delta s_{ii} = 2G\left[\Delta\varepsilon_{ii} - \frac{1}{3}\frac{\Delta V}{V}\right]; \quad \Delta s_{ij} = 2G\Delta\varepsilon_{ij} \tag{2}$$

where G is shear modulus, Δs_{ij} is the deviatoric stress increment, $\Delta\varepsilon_{ij}$ is the strain increment and $\Delta V/V$ is the relative change in volume which can be determined by equation of state.

The dynamic strength surface is amplified from static surface by considering the strain rate effect. Typically the compressive (tensile) strength is multiplied by a compressive (tensile) DIF. In the model, the DIF of the compressive strength is from the CEB recommendation (Bischoff and Perry, 1991). The DIF for tensile strength is obtained from curve fitting the available experimental results as follows,

$$TDIF = f_{td} / f_{ts} = 1.0 \quad \text{for } \dot{\varepsilon}_d \le 10^{-4} s^{-1} \tag{3a}$$

$$TDIF = f_{td} / f_{ts} = 2.06 + 0.26\log\dot{\varepsilon}_d \quad \text{for } 10^{-4} s^{-1} \le \dot{\varepsilon}_d \le 1s^{-1} \tag{3b}$$

$$TDIF = f_{td} / f_{ts} = 2.06 + 2\log\dot{\varepsilon}_d \quad \text{for } \dot{\varepsilon}_d > 1s^{-1} \tag{3c}$$

where $\dot{\varepsilon}_d = \sqrt{(2/3)\dot{\varepsilon}_{ij}\dot{\varepsilon}_{ij}}$ is the equivalent strain rate, $\dot{\varepsilon}_{ij}$ is the strain rate tensor. It should be noted that the highest cut-off strain rate considered is $1000s^{-1}$ to avoid overestimation of the strain rate effect.

The piece-wise Drucker-Prager yield strength model (shown in Figure 2) is

$$F_p = \sqrt{J_2} - b_i p - a_{id} \le 0 \quad (i = 1 \sim N) \tag{4}$$

where $J_2=1/2 s_{ij}s_{ij}$, is the second invariant of the stress deviator tensor s_{ij}; p is the hydro-pressure; $a_{id}=a_i(1-D)$; D is a damage scalar, which will be discussed later; a_i and b_i are the material constants which can be determined by four sets of experimental data: (1) the cut off hydro-tensile strength f_{ttt}, ($f_{ttt} = \sigma_1 = \sigma_2 = \sigma_3$, point 1 in Figure 2, the value is obtained based on Kotsovos(1995)' meridian curve); (2) the uniaxial tensile strength f_t; ($f_t = \sigma_1$, $\sigma_2 = \sigma_3 = 0$, point 2 in Figure 2); (3) the uniaxial compressive strength f_c ($\sigma_1 = \sigma_2 = 0$, $\sigma_3 = -f_c$, point 3 in Figure 2); and (4) the confined compressive strength ($I_1 = 10\sqrt{3} f_c$, $\sqrt{2J_2} = 6 f_c$, point 4 in Figure 2, where I_1 is the first stress invariant; J_2 is the second deviatoric stress invariant. These values are based on a review of the test results on the compression meridian published in a textbook by Chen (1982)). Once the yield surface defined by Eq (4) is reached, the material has permanent plastic strain. The details on the plastic flow treatment in AUTODYN can be found in its theory manual (AUTODYN, 2005). The damage scalar D can be determined by the Mazars (1986)' damage model,

$$D = A_t D_t + A_c D_c, \quad \dot{D}_t > 0, \quad \dot{D}_c > 0, \quad \text{and} \quad A_t + A_c = 1 \tag{5}$$

The tensile damage D_t and the compressive damage D_c are

$$D_t(\tilde{\varepsilon}_t) = 1 - e^{-\alpha_t(\tilde{\varepsilon}_t - \varepsilon_{t0})/\varepsilon_{t0}} \qquad D_c(\tilde{\varepsilon}_c) = 1 - e^{-\alpha_c(\tilde{\varepsilon}_c - \varepsilon_{c0})/\varepsilon_{c0}} \tag{6}$$

where α_t and α_c are damage parameters and both are taken as 0.5, while ε_{to} and ε_{co} are the threshold strains in uniaxial tensile and compressive states, they are assumed to be strain rate sensitive, that is, $\varepsilon_{to}=TDIF\times\varepsilon_{sto}$, $\varepsilon_{co}=CDIF\times\varepsilon_{sco}$, in which ε_{sto} and ε_{sco} are the static tensile threshold strain in uniaxial tension and compression.; $\tilde{\varepsilon}_t$ and $\tilde{\varepsilon}_c$ are the equivalent tensile and compressive strains, defined as $\tilde{\varepsilon}_t = \sqrt{\sum_{i=1,3} \left(\varepsilon_i^+\right)^2}$, $\tilde{\varepsilon}_c = \sqrt{\sum_{i=1,3} \left(\varepsilon_i^-\right)^2}$ where ε_i^+ is the positive principal strain. The '+' means it vanishes if it is negative. ε_i^- is negative principal strain, and the '–' means it vanishes if it is positive. The weights A_t and A_c in Eq(5) are defined by the following expressions,

$$A_t = \sum_{i=1,3} \frac{H_i\left[\varepsilon_i^+\left(\varepsilon_i^+ + \varepsilon_i^-\right)\right]}{\tilde{\varepsilon}^2}, \quad A_c = \sum_{i=1,3} \frac{H_i\left[\varepsilon_i^-\left(\varepsilon_i^+ + \varepsilon_i^-\right)\right]}{\tilde{\varepsilon}^2} \tag{7}$$

where $\tilde{\varepsilon} = \sqrt{\sum_{i=1,3} \left(\varepsilon_i^+ + \varepsilon_i^-\right)^2}$ is the effective strain. $H_i[x]=0$ when x < 0 and $H_i[x]=x$ when $x \geq 0$.

When the concrete material is under compression ($p>0$), the maximum D_{max} needs to be set to allow some residual strength. It is well accepted by many researchers (Riedel et al., 1999, Holmquist and Johnson, 1993, Gebbeken and Rippert, 2000) that the fully damaged concrete (or granular material) can still sustain a portion of shear stress. This phenomenon can be explained as friction resistance. In Johnson-Holmquist model (Holmquist and Johnson, 1993) and RHT model (Riedel et al., 1999), this part is assumed to be $\sigma^* = BP^{*N}$, where B and N are material constants, P^* is the normalized pressure. In Gebekken's model (Gebbeken and Rippert, 2000), the residual strength is assumed to be 33.8% of the compressive strength. So far the phenomenon of the friction resistance is still not well understood, and there is no test result available to determine the residual strength. In order not to overestimate this strength, in the present study, a relatively lower portion of strength, that is 20% of the compressive strength, is assumed as the residual capacity. For more detail description of this model, readers are referred to reference (Zhou et al., 2008).

3 Calibration of the concrete model

Figure 3 shows a sketch of the RC slabs tested in the Weapons System Division, Defence Science and Technology Organisation, Department of Defence, Australia. They are used to calibrate the model described above. The concrete compressive strength of the slabs is 50MPa. The cover for the reinforcement bars is about 20mm. As shown, a steel frame was used to mount the concrete slab. A cardboard box on the top of the slab is used as a disposable pedestal for the cylindrical explosive. Explosive charges of CompB and Powergel were used. The CompB charge was in a cylindrical shape, weighing about 0.5kg; the Powergel charge consisted of 3 slurry sticks with a total weight similar to the CompB charge. The charge was positioned as shown in Figure 3.

In numerical model, air is modelled by an ideal gas equation of state. The standard constants of air from AUTODYN (2005) material library are used. High explosives (TNT) are typically modelled by using the Jones-Wilkins-Lee (JWL) equation of state. The hydrostatic pressure p is determined by the specific internal energy e and specific volume v as follows,

$$p = C_1\left(1-\frac{\omega}{r_1 v}\right)e^{-r_1 v} + C_2\left(1-\frac{\omega}{r_2 v}\right)e^{-r_2 v} + \frac{\omega e}{v} \tag{8}$$

where C_1, r_1, C_2, r_2 and ω are material constants. For explosive charge CompB, C_1, r_1, C_2, r_2, and ω are 3.7377×10^5MPa, 4.15, 3.7471×10^3MPa, 0.9, 0.35, respectively; while for the Powergel, they are 4.976×10^4MPa, 3.907, 1.891×10^3MPa, 1.118 and 0.3333.

In the test, the RC slab is placed on shape steels at two ends to make it work as a one way slab. Each boundary end has a width of 100mm as shown in Figure 3. It is assumed that the concrete slab is directly placed on the supports because the uplift movement is not fixed. The reinforcement bars are modeled by an elastoplastic steel model, in which the yield stress and Young's modulus are assumed to be 310MPa and 200GPa, respectively. It should be noted that the Johnson Cook model was also used in the simulation. It was found that there is no difference because all the steel bars are still in elastic stage.

In the numerical calculation, 2D fine mesh is used initially to simulate blast wave propagation. The 2D simulation results are remapped to 3D model when blast wave reaches the concrete slab. In the 3D model, the interaction between the blast wave propagation in Euler subgrid and the solid Lagrange RC subgrid is considered. Both reinforcement and concrete are modelled by solid elements; perfect bond is assumed. The element size in the 2D model is $1\times1mm^2$. In the central area of the 3D slab model, that is, within an area of $500\times500mm^2$, the element size is $4\times4\times4mm^3$ for concrete, steel, air and the high explosive. The mesh size increases gradually away from the slab centre. The total element number in the 3D model is 646,000. The parameters for concrete strength model are given in Table 2.

In the numerical simulation, the dynamic loading acted on the concrete surface can be obtained by considering the interaction between the Euler elements and the Lagrange elements. The Lagrange elements impose geometric constraints on the Euler elements while the Euler elements provide a pressure boundary to the Lagrange elements. This pressure boundary, i.e., the reflected pressure-time history is recorded during the calculation. The numerical peak reflected pressures are compared with those obtained from the empirical method in TM5-1300 (1990). In order to check the value in TM5-1300, the TNT equivalency ratio needs to be determined first. According to Table 2-1 in TM5-1300 (1990), the TNT equivalency ratio for CompB is 1.09; and the TNT equivalency ratio for Powergel is about 0.8 based on

the information the supplier provided. From the empirical chart in TM5-1300, the peak reflected pressure for the CompB charge case can be estimated as 215MPa. In the numerical simulation, the recorded peak reflected pressure is 206MPa. The numerical result agrees well with that from the empirical result with a deviation of 4.2%. The empirical peak pressure for the Powergel charge case is about 152MPa, while the numerical pressure is 128MPa with a deviation of 15.8%. The calculated impulses are also compared with these obtained from TM5-1300, the deviations are less significant as compared to the peak pressure.

For the CompB charge case, the comparison of the damaged areas obtained from the numerical simulation with those from the test is shown in Figure 4. From this figure, it can be found that: 1) in the numerical simulation (Figure 4 a) there is a small damaged area at the center of the slab surface, which is compressive damage; 2) there is also a small indentation in the center area, which is caused by the high pressure from the explosion (Figure 4 b); 3) the calculated damaged area on the bottom surface of the slab shown in Figure 4 c has a similar shape and area with that in the test (Figure 4 d). The area of the rectangular marked in Figure 4 c and d has the same size of $480\times300mm^2$. It was observed that spalling occurred in the test. The maximum depth of the cavity at the center is about 50mm. While in the numerical simulation, the depth of the damaged part at the center is 44mm, which is slightly lower than the experimental cavity depth.

For the Powergel charge case, the comparison of the damaged areas obtained from the numerical simulation with those from the test is shown in Figure 5. Numerical results show that there is no damage on the upper side of the slab, which is consistent with the test results shown in Figure 5 (b). On the bottom surface of the slab, a small damaged area with a relatively low damage value can be found in the center of the slab as shown in Figure 5 (c). Similarly there are some cracks near the center of slab in Figure 5 (d).

These comparisons demonstrate that the numerical model gives reasonable prediction of RC slab response to blast loads.

4 Simulation and results

4.1 Typical RC wall setup

Figure 6 shows a RC wall in a typical building for office or residential use. The dimension of the wall is 3400×3500×300mm^3. On each side, the vertical and longitudinal reinforcement is ∅16@150mm, and the transverse reinforcement is ∅16@200mm. Therefore, the reinforcement ratio in the wall is about 1.5%.

4.2 Numerical simulation of the RC wall response

The finite element model is shown in Figure 7. Four front layers of concrete elements are removed to show the reinforcement. The mesh includes 68×140×20 brick concrete elements and 2 layers of beam elements for reinforcement. Both the concrete and the steel are assumed to have the same respective parameters as those in the calibration test (the material parameters for concrete strength are given in Table 2). As shown in Figure 6, explosion is assumed to take place on ground surface at a stand-off distance. Only one half of the RC wall is modelled because of symmetry. In the simulation, the boundary is assumed to be fixed.

Because the duration of the blast wave is extremely short, structures usually have no time to deform significantly during the action of blast wave. Therefore the blast wave-structure interaction effect is normally insignificant. In common blast effect analysis and design, the blast wave-structure interaction effect is neglected, i.e., the reflected blast pressure is applied to the structure surface as external dynamic loads without considering the blast wave propagation (TM5-1300, 1990). Moreover, including blast wave-structure interaction in the 3D numerical model substantially increases the computational effort. Because of the limitations of the computer memory and software capacity, bigger mesh sizes often have to be used if blast wave-structure interaction is modelled. For example, for the problem under consideration in this study, if blast wave-structure interaction is modelled in the 3D simulation, the smallest mesh size that can be adopted is 25 mm for the stand-off distance of 2m (it is 65mm when the stand-off distance is 10m), whereas it is 15 mm for all cases if the interaction is not modelled. Modelling the interaction with a big mesh size may lead to more significant numerical errors than neglecting the interaction. For these reasons, the blast wave-structure interaction is not modelled. In this study, the

reflected pressure-time histories are obtained with a fine mesh size in an axi-symmetric simulation first, and then applied to the RC wall as external dynamic loads to calculate the response and damage.

In numerical simulations, a series of stand-off distances are considered. At each stand-off distance, likely charge weights as described above are used to carry out the numerical simulation of RC wall responses. The pressure time histories at different gauge points on the surface of RC wall derived from AUTODYN 2D simulation are used as input on the respective surface areas of the wall. One of the 2D models is shown in Figure 8. The wall surface is assumed as rigid to get the blast loading. The pressure time histories on these gauge points are recorded. Figure 8 b is a typical pressure-time history at gauge point A for D=10m, w=500kg. In order to accurately input the blast loading, the wall surface is divided into 5 different pressure areas as shown in Figure 9. The loading on each area is set as the same as the recorded pressure at the corresponding gauge point. The peak reflected pressure and impulse are compared with that obtained from TM5-1300 (1990), as shown in Table 3. From this table, it can be found that most of the peak reflected pressures obtained from AUTODYN are higher than that obtained from TM5-1300 with a deviation up to 15%; and for all the cases, the impulses obtained from AUTODYN 2D are higher than that of TM5-1300 with a deviation up to 23%. Because the latter is based on a large amount of test results, the calculated response in the present study may be over estimated. It should be noted that in most design and analysis of structure wall response to blast loads, the pressure is usually assumed as uniform over the entire wall. This assumption is acceptable if the stand-off distance is relatively large and the blast wave front is plane. It may lead to inaccurate prediction of wall response to blast load if explosion center is near the wall. The current study that divides the wall into five zones in estimating the blast loadings on the wall will yield more accurate prediction of wall responses than the uniform pressure distribution assumption.

In the present study, the damage condition of the RC wall can be divided into four levels: 1) no damage: from initial state to some slight cracks (in numerical simulation this corresponds to a small damage area with a low damage value); 2) slight damage: from a few cracks to crushing or spalling damage up to one third of the wall thickness, and the reinforcement bars are still in elastic stage, usually there is no damage on the front surface; 3) moderate damage: crush and spall depth from one third of the wall thickness to almost perforation, in this case normally it can be found that the steel bars in a small

area near the centre are in the plastic range, sometimes compressive damage can be found on the front surface; 4) severe damage: for damage more severe than fully perforation, large portion of steel bars are in the plastic region. It should be mentioned that the present damage levels can be related to different protection levels. Only the damage level (4) can be considered as structural failure with low protection level. Similar damage categories can also be found in (Xu and Lu, 2006). It should also be noted that these damage definitions are subjective. This is because 1) the definition of damage level of a structure is usually fuzzy; 2) the damage scalar defined in this numerical model is based on the theory of continuum mechanics, which does not explicitly differentiate the crack propagation and spalling, although it predicts damage propagation. The correlation between the damage scalar and concrete damage used in this study is based on the comparison between numerical simulations and test results in the calibration study. The spalling depth and the perforation are estimated from the damage level across the wall depth. When the damage level is higher than 0.99 for all the elements across the RC wall depth, it is assumed that the perforation occurs.

Typical slight damage, moderate damage and severe damage scenarios for the RC wall in Figure 6 are shown in Figure 10. For slight damage and moderate damage, normally there is no or only small damaged area can be found in the front surface besides the damage at the back surface, while for the severe damage case, large damaged area can also be found on the front surface because the high pressure can directly crush the concrete (as shown in Figure 10 e). From the numerical results, it can also be found that: when the charge is near the RC wall, i.e., the stand-off distance is 2m, the severe damage area is at the lower part of the wall because the pressure varies significantly in different part of the wall surface (as shown in Figure 10 b). When the stand-off distance is larger than 5m, the pressure-time history in different area does not vary significantly. Therefore, the RC wall is under almost a uniformly distributed loading (as shown in Figure 10 c to f).

Based on the numerical results, some critical charge weight – stand-off distance relationships are constructed in Figure 11. The first curve determined is the threshold curve from no damage to small damage, the relationship between the stand-off distance to the charge weight can be approximated as,

$$R = 5.2\ln(w) - 12.5 \quad (2m \le R \le 20m) \tag{9}$$

where R is the stand-off distance in meters, w is the charge weight in kg. Any combination of R and w on the left of this curve means that no damage will occur. The second curve is the critical curve from slight damage to moderate damage, which can be determined by,

$$R = 5.6\ln(w) - 20.1 \qquad (2m \le R \le 20m) \tag{10}$$

For those points between the first curve and the second curve, slight damage is expected. The third curve divides the moderate damage and the severe damage, which is

$$R = 6.0\ln(w) - 28.3 \qquad (2m \le R \le 20m) \tag{11}$$

Any point at the right side of the third curve means that the combination of R and w will cause severe damage to the RC wall considered in this study. It should be noted that the three curves are only suitable for the stand-off distance ranging between 2m and 20m. In Figure 11, the scattered points are the numerical results obtained in the present study. FEMA (2008)'s threshold line for failure of concrete columns is also given for comparison. It can be found that FEMA's line is close to the third curve when the charge weight is higher than 1000kg. However, when the charge weight is lower, FEMA suggested stand-off distance is much higher than Eq. (11). From this figure, it is clear that for a truck bomb, the safe stand-off distance to avoid severe damage should be at least 20m, while for a van bomb, the safe stand-off distance is around 10m. It should be noted that this results are obtained based on the particular RC wall analysed in this study. More analyses are needed on RC walls of different dimensions, different reinforcement ratios, and different boundary conditions in order to derive a more general formula for a quick assessment of the RC wall performance to blast loads.

5 Conclusions

A dynamic plastic damage model for concrete developed in a previous paper has been adopted to predict the damage of a reinforced concrete wall under blast loading in the present study. Numerical simulations of the dynamic responses of a typical RC wall to many different cases of blast loadings have been carried out. The dynamic blast loading is derived from the AUTODYN 2D simulation. Comparison between the numerical results and the empirical chart in TM5-1300 shows that the peak pressure and impulse of the simulated pressure time histories agree well. The largest difference between the numerical

simulation and the empirical prediction from TM5-1300 is about 23%. The simulated pressure time histories are used as input to the 3D model to calculate the response and damage of the RC wall to blast loads. Based on the numerical results, critical curves corresponding to different damage levels have been derived. From the critical curves, it is clear that for the RC wall considered in this study, if a truck bomb of 3000kg occurs, the safe stand-off distance to avoid severe damage is about 20m, whereas for a van bomb of 600kg, the safe stand-off distance is about 10m. The derived analytical formulae allows for a quick assessment of the RC wall performance under blast loadings. To derive the more general analytical formulae, more simulations are needed with RC walls of different dimensions, different reinforcement ratios, and different boundary conditions

Acknowledgements

The authors would like to thank the Australian Research Council for partial financial support under grant no. DP0774061 to carry out this research work, and thank Drs John Waschl and Valerian Kuznetsov from DSTO Australia for providing testing results for calibration of the numerical model.

References

Ambrosini, D., Luccioni, B., Jacinto, A. and Danesi, R. (2005). “Location and mass of explosive from structural damage”, *Engineering Structures*, Vol. 27, pp.167-176.

AUTODYN (2005), Century Dynamics, Theory manual.

Bischoff, P.H. and Perry, S.H. (1991). “Compressive behaviour of concrete at high strain rate”, *Materials and Structures*, Vol. 24 pp.425-50.

Chen, A.C.T. and Chen, W.F. (1975). “Constitutive relations for concrete”, *Journal of Engineering Mechanics Division, ASCE,* Vol. 101(EM4), pp.465-81.

Chen, W.F. (1982). *Plasticity in Reinforced Concrete*, McGraw Hill, New York.

Department of Defense (DOD). (2005). *Unified Facilities Criteria (UFC) design of buildings to resist progressive collapse,* UFC 4-023-03, Washington, D.C.

Department of Defense (DOD). (2002). *Unified Facilities Criteria (UFC), DOD Minimum Antiterrorism Standard for Buildings*, UFC 4-010-01, 31 July. Washington, D.C.

Eibl, J. and Schmidt-Hurtienne, B. (1999). “Strain-rate-sensitive constitutive law for concrete”, *Journal of Engineering Mechanics, ASCE, Vol.*125, No.12, pp.1411-20.

Espinosia, H.D., Zavattieri, P.D. and Dwivedi, S.K. (1998). “A finite deformation continuum/discrete model for the description of fragmentation and damage in brittle material”, *Journal of the Mechanics and Physics of solids*, Vol.46, pp.1909-42.

FEMA 428 (2008). *Explosive blast*. Online available from: http://www.wbdg.org/ccb/FEMA/fema428.pdf.

Fu, H.C., Erki, M.A. and Seckin, M. (1991). “Review of effects on loading rate on concrete in compression”, *Journal of Structural Engineering*, ASCE, Vol.117, No.12, pp.3645-59.

Gatuingt, F. and Pijaudier-Cabot, G. (2002). “Coupled damage and plasticity modelling in transient dynamic analysis of concrete”, *International Journal for Numerical and Analytical Methods in Geomechanics*, Vol.26, pp.1-24.

Gebbeken, N., Greulich, S. and Pietzsch A. (2006). “Hugoniot properties for concrete determined by full-scale detonation experiments and flyer-plate-impact tests”, *International Journal of Impact Engineering*, Vol.32, pp.2017-2031

Gebbeken, N. and Ruppert, M. (2000). A new material model for concrete in high-dynamic hydrocode simulations. *Archive of Applied Mechanics*, Vol.70, pp.463-78.

Herrmann, W. (1969). Constitutive equation for the dynamic compaction of ductile porous materials, Journal of applied physics, Vol.40, pp.2490-9.

Holmquist, T.J. and Johnson, G.R. (1993). “A Computational Constitutive Model for Concrete Subjected to Large Strains, High Strain Rates, and High Pressures”, *Proceedings of the 14th International Symposium on Ballistics*, Quebec, Canada , pp.591-600.

Kotsovos, M.D. and Newman, J.B. (1978). “Generalised stress-strain relations for concrete, Journal of Engineering Mechanics Divisions, ASCE, Vol.104(EM4), pp.845-56.

Kotsovos, M.D. and Pavlovic, M.N.(1995), *Structural Concrete, Finite Element Analysis for Limit State Design.* Published by Thomas Telford Publications, London.

Lan, S. and Crawford, J.E. (2003). “Evaluation of the blast resistance of metal deck roofs”, *The 5th Aisa-Pacific Conference on Shock & Impact Loads on Structures,* 12-14 November, Changsha, Hunan, China. pp.213-220.

Leppänen, J. (2006). “Concrete subjected to projectile and fragment impacts: Modeling of crack softening and strain rate dependency in tension”, *International Journal of Impact Engineering*, Vol.32 pp.1828-1841.

Li, Q.M. and Meng, H. (2002). “Pressure-impulse diagram for blast loads based on dimensional analysis and single-degree-of freedom model”, *Journal of Engineering Mechanics*, Vol.128, No.1, pp.87-92.

Malvar, L.J., Crawford, J.E., Wesevich, J.W. and Simons, D. (1997). “A plasticity concrete material model for DYNA3D”. *International Journal of Impact Engineering,* Vol.19, pp.847-873.

Malvar, L.J. and Ross, C.A. (1998). “Review of strain rate effects for concrete in tension”, *ACI Materials Journal*, Vol.95(M73), pp.735-9.

Mazars, J. (1986). “A description of micro- and macroscale damage of concrete structures”, *Engineering Fracture Mechanics*, Vol.25, No.5/6, pp.729-737.

Morison, C.M. (2006). “Dynamic response of walls and slabs by single-degree-of-freedom analysis —a critical review and revision”, *International Journal of Impact Engineering*, Vol.32, pp.1214-1247.

Mosalam, K.M. and Mosallam, A.S. (2001). “Nonlinear transient analysis of reinforced concrete slabs subjected to blast loading and retrofitted with CFRP composites”, *Composites: Part B,* Vol.32, pp.623-636.

Naito, C.J. and Wheaton, K.P. (2006). “Blast assessment of load-bearing reinforced concrete shear walls”, *Pratice Periodical on Structural Design and Construction*, Vol.11, No.2, pp.112-121.

Ottesen, N.S. (1977). “A failure criteria for concrete”, J*ournal of the engineering Mechanics Division*, ASCE, Vol.103(EM4), pp.527-535.

Pinto, P.E. (1996). *RC Elements Under Cyclic Loading, State of the Art Report.* Thomas Telford, London.

Rabczuk, T. and Eibl, J. (2003). “Simulation of high velocity concrete fragmentation using SPH/MLSPH”, *International Journal of Numerical Methods in Engineering, Vol.*56, pp.1412-1444.

Riedel, W., Thoma, K., Hiermaier, S. and Schmolinske, E. (1999). “Penetrating of reinforced concrete by BETA-B-500 numerical analysis using a new macroscopic concrete model for hydrocodes”, *Proceedings of 9th International Symposium IEMS*, Berlin, pp.315-322.

Schuler, H., Mayrhofer, C. and Thoma, K. (2006). “Spall experiments for the measurement of the tensile strength and fracture energy of concrete at high strain rates”, *International Journal of Impact Engineering*, Vol.32, pp.1635-1650.

TM5-1300. (1990). *Structures to resist the effects of accidental explosions.* US army. USA.

Xu, K. and Lu, Y. (2006). “Numerical simulation study of spallation in reinforced concrete plates subjected to blast loading”, Computers and Structures, Vol.84, pp.431-438.

Zhou, X.Q., Hao, H. and Deeks AJ. (2005). “Modelling Dynamic Damage of Concrete Slab under Blast Loading” *Proceedings of the 6th International Conference on Shock & impact Loads on Structures,* Perth, Australia, 7-9, December, pp.703-10.

Zhou, X.Q., Kuznetsov, V., Hao, H. and Waschl, J. (2008). “Numerical calculation of concrete slab response to blast loading”, *Special Issue of the international Journal of Impact and Engineering*, accepted, will be on line soon.

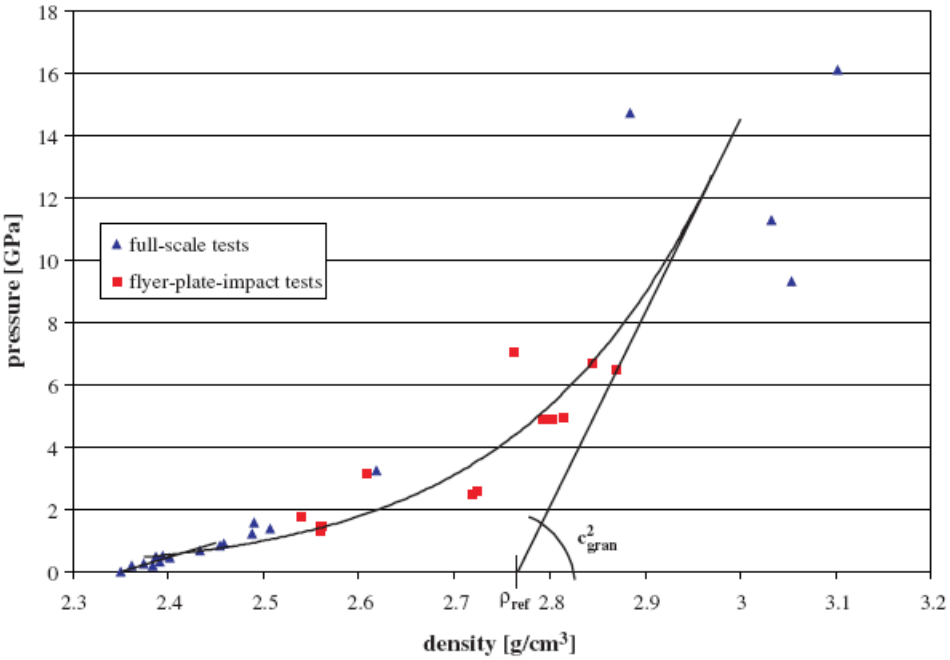

Figure 1. Typical Pressure-density relationship in EOS (Gebbeken et al., 2006)

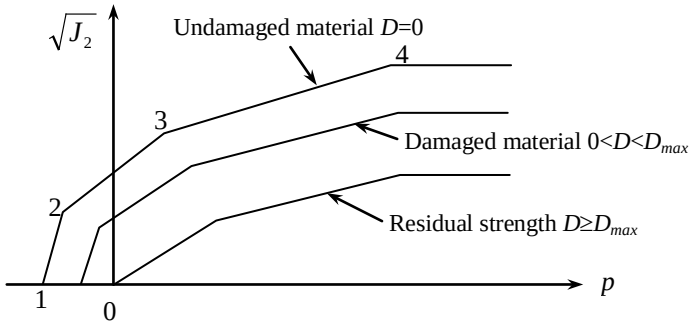

Figure 2. Damage-dependent piece-wise Drucker-Prager strength criterion

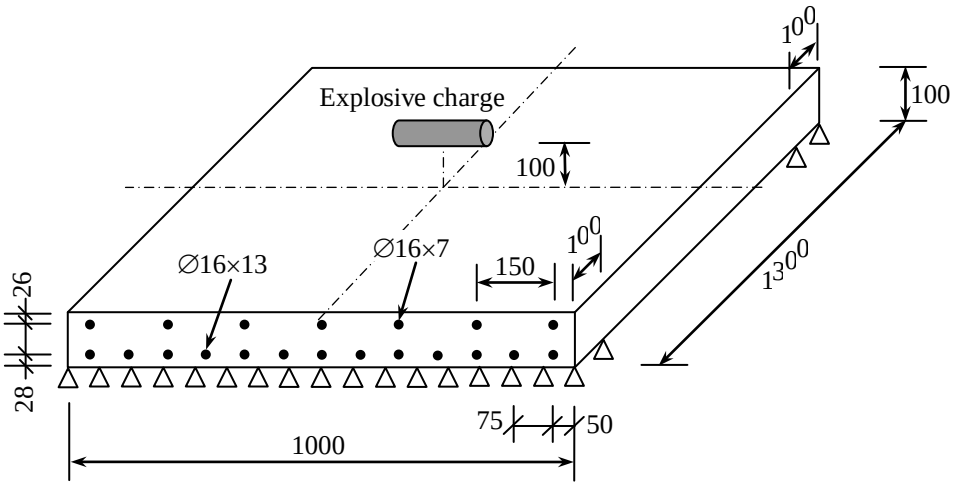

Figure 3. Details of the RC slab

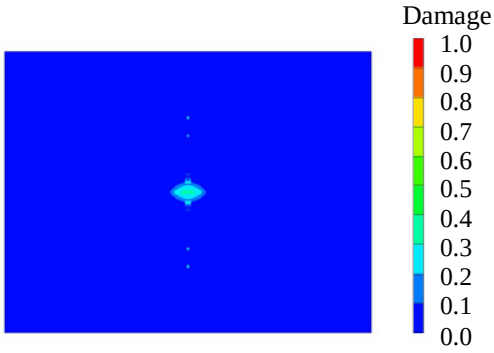

(a) Numerical prediction (upper face)

(b) Experimental results (upper face)

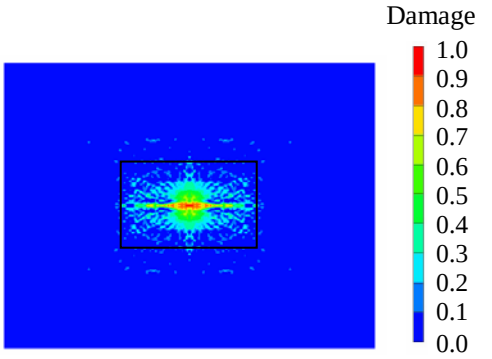

(c) Numerical prediction (bottom face)

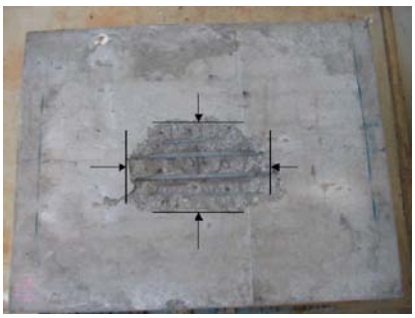

(d) Experimental results (bottom face)

Figure 4. Comparison of the numerical results and the experimental results (Comp B)

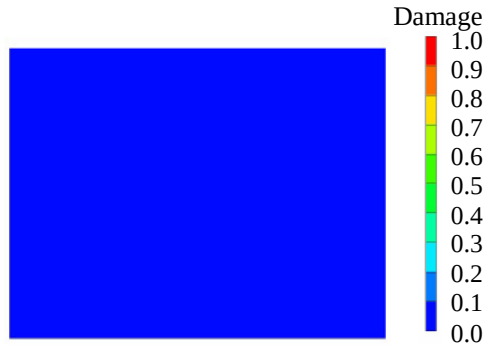

(a) Numerical prediction (upper face)

(b) Experimental results (upper face)

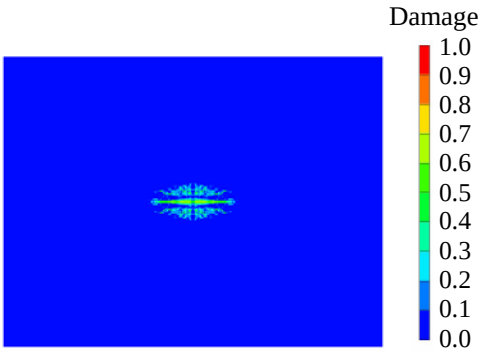

(c) Numerical prediction (bottom face)

(d) Experimental results (bottom face)

Figure 5. Comparison of the numerical results and the experimental results (Powergel)

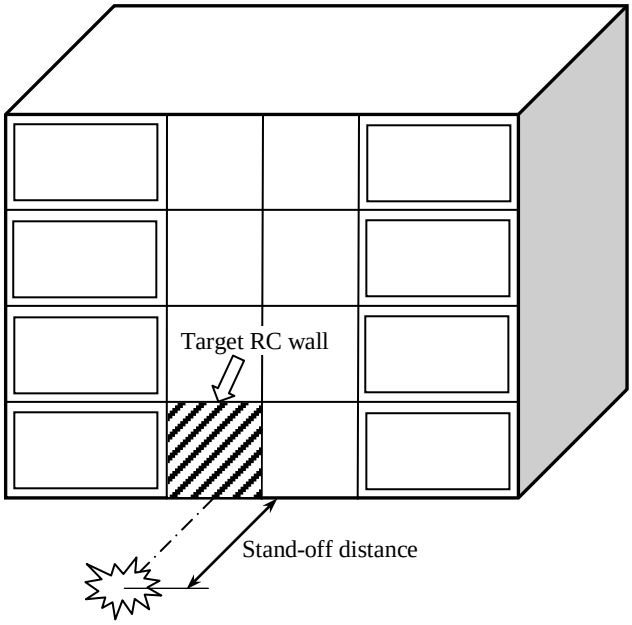

Figure 6. Typical RC wall in a building

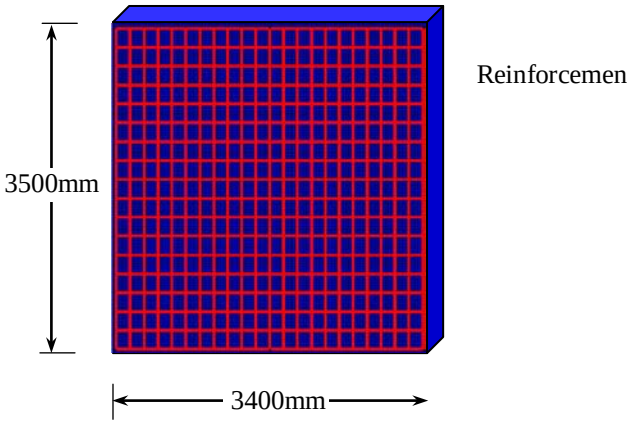

Figure 7. Finite elment model of the target RC wall

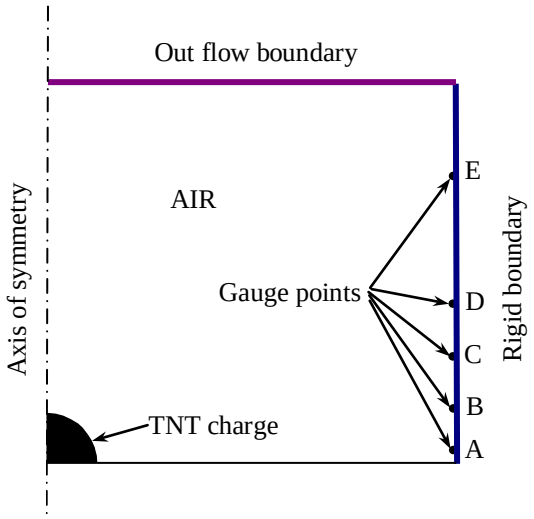

a) 2D numerical model

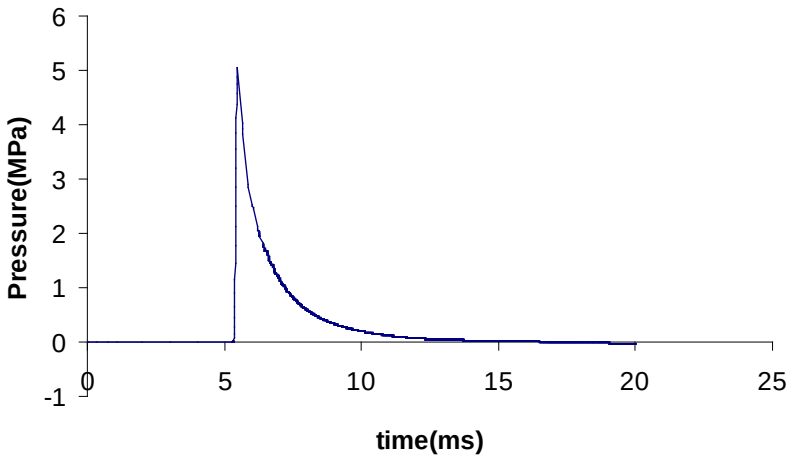

b) Pressure time history on gauge point A (W=500kg, R=10m)

Figure 8. 2D numerical model and typical pressure-time history on a gauge point

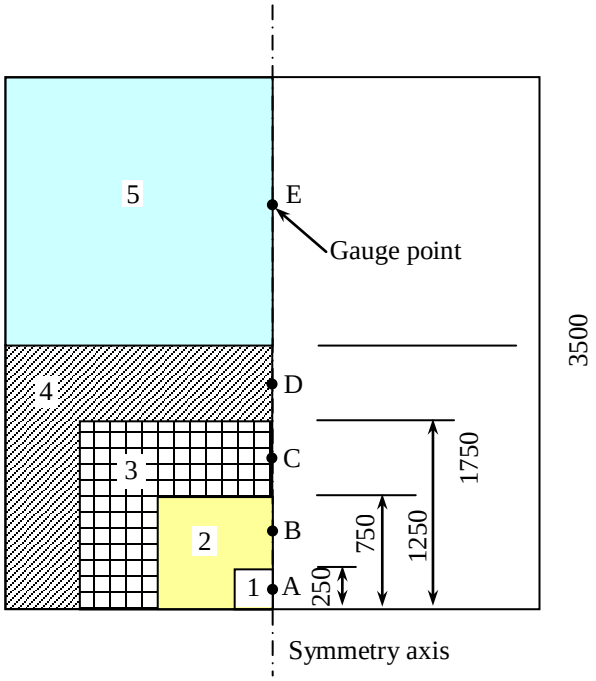

Figure 9 Areas for different pressure time history (mm)

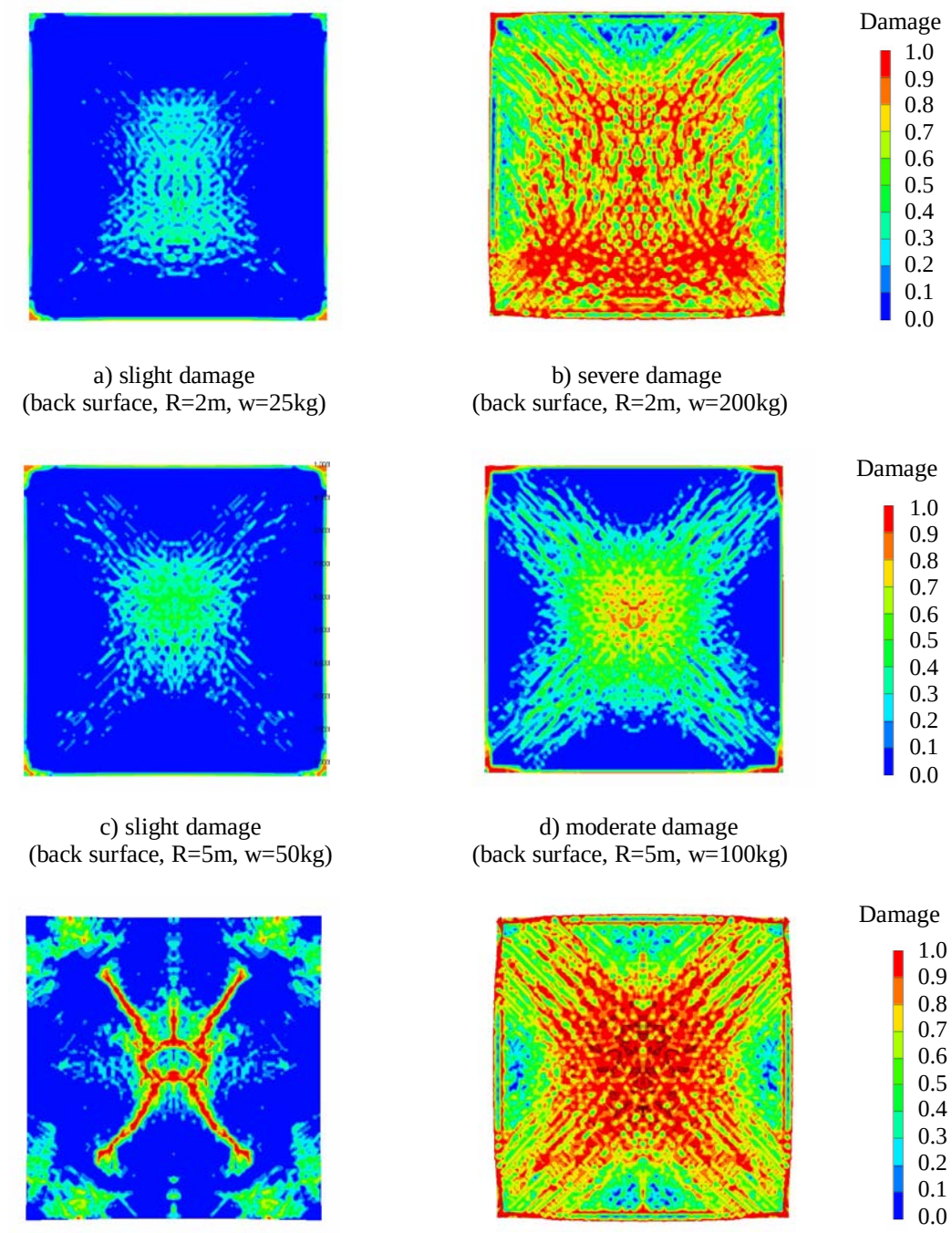

a) slight damage
(back surface, R=2m, w=25kg)

b) severe damage
(back surface, R=2m, w=200kg)

c) slight damage
(back surface, R=5m, w=50kg)

d) moderate damage
(back surface, R=5m, w=100kg)

e) severe damage
(front surface, R=20m, w=5000kg)

f) severe damage
(back surface, R=20m, w=5000kg)

Figure 10. Typical damage contour for slight damage, moderate damage and severe damage

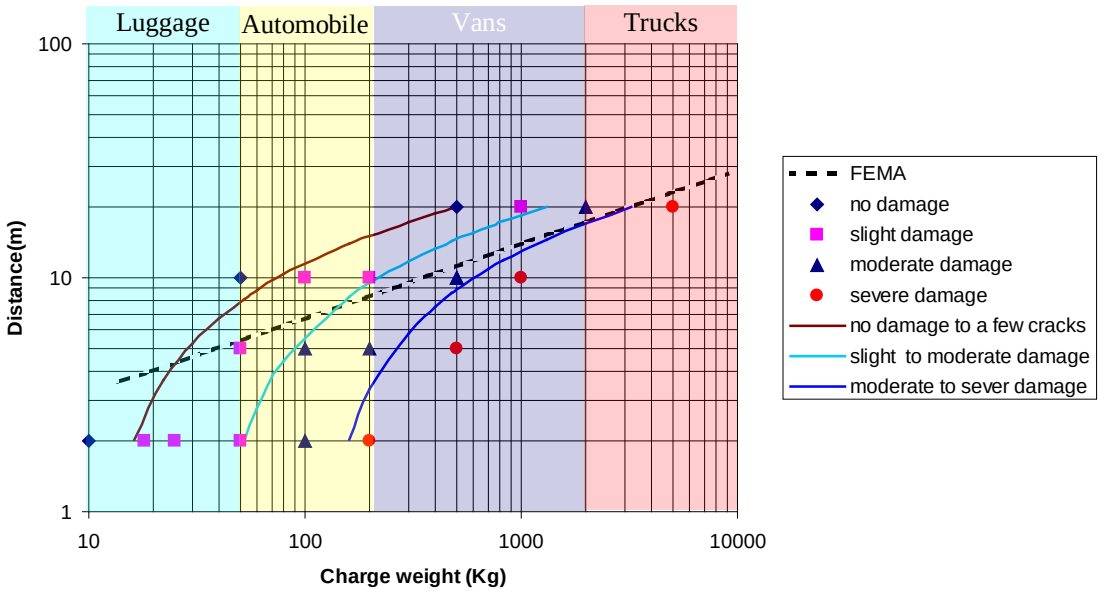

Figure 11 Critical charge weight – stand-off distance for different damage level

Table 1 Material constants for EOS of concrete

Solid density ρ_s	2.750×10^3kg/m^3	A_2	3.958×10^4MPa
Initial densityρ_0	2.314×10^3kg/m^3	A_3	9.04×10^3MPa
Initial soundspeed C_0	2.920×10^3m/s	B_0	1.22
Initial compaction pressure p_e	23.3MPa	B_1	1.22
Solid compaction pressure p_s	6000MPa	T_1	1.513×10^5MPa
Polynomial EOS parameters A_1	1.513×10^5MPa	T_2	0

Table 2 Material constants for concrete strength model

α_t, α_c	ε_{st0}	ε_{sc0}	f_t	f_c	f_{ttt}
0.5	$3.5e^{-4}$	$3.5e^{-3}$	4MPa	50MPa	2MPa

Table 3 Peak reflected pressure and impulse on the RC wall

Charge weight (kg)	Distance (m)	Scaled distance ($m/kg^{1/3}$)	TM5-1300		Numerical results (AUTODYN)		Deviation	
			Peak pressure (MPa)	Impulse (MPa·ms)	Peak pressure (MPa)	Impulse (MPa·ms)	Peak pressure	Impulse
10	2	0.928	9.93	2.11	9.34	2.17	-6.32%	2.76%
18	2	0.763	16.70	3.36	15.50	3.56	-7.74%	5.62%
25	2	0.684	20.75	4.38	21.47	4.80	3.35%	8.75%
50	2	0.543	33.67	7.72	29.60	8.30	-13.75%	6.99%
100	2	0.431	51.99	13.80	50.16	16.52	-3.65%	16.46%
200	2	0.342	77.79	24.99	68.95	32.50	-12.82%	23.11%
50	5	1.357	3.42	2.18	3.99	2.44	14.29%	10.66%
100	5	1.077	6.65	3.71	7.64	4.08	12.96%	9.07%
200	5	0.855	12.24	6.40	13.29	6.80	7.90%	5.88%
500	5	0.630	24.82	13.38	25.6	14.7	3.05%	8.98%
50	10	2.714	0.43	0.93	0.51	1.11	15.69%	16.22%
100	10	2.154	0.85	1.54	0.97	1.88	12.37%	18.09%
200	10	1.710	1.70	2.58	1.97	3.07	13.71%	15.96%
500	10	1.260	4.25	5.17	5.04	5.73	15.67%	9.77%
1000	10	1.000	8.15	8.85	9.41	10.1	13.39%	12.38%
500	20	2.520	0.54	2.19	0.61	2.66	11.48%	17.67%
1000	20	2.000	1.06	3.64	1.21	4.43	12.40%	17.83%
2000	20	1.587	2.13	6.10	2.49	7.20	14.46%	15.28%
5000	20	1.170	5.27	12.28	6.19	13.50	14.86%	9.04%